Mercury isotopes of atmospheric particle bound mercury for source apportionment study in urban Kolkata, India

Reshmi Das[1*] • Xianfeng Wang[1,2] • Bahareh Khezri[3] • Richard D. Webster[3] • Pradip Kumar Sikdar[4] • Subhajit Datta[5]

[1]Earth Observatory of Singapore, Nanyang Technological University, Singapore
[2]Asian School of the Environment, Nanyang Technological University, Singapore
[3]Division of Chemistry and Biological Chemistry, School of Physical and Mathematical Sciences, Nanyang Technological University, Singapore
[4]Department of Environment Management, Indian Institute of Social Welfare and Business Management, Kolkata, India
[5]Information Systems Technology and Design, Singapore University of Technology and Design, Singapore

*reshmidas@ntu.edu.sg

Abstract

The particle bound mercury (PBM) in urban-industrial areas is mainly of anthropogenic origin, and is derived from two principal sources: Hg bound to particulate matter directly emitted by industries and power generation plants, and adsorption of gaseous elemental mercury (GEM) and gaseous oxidized mercury (GOM) on air particulates from gas or aqueous phases. Here, we measured the Hg isotope composition of PBM in PM_{10} samples collected from three locations, a traffic junction, a waste incineration site and an industrial site in Kolkata, the largest metropolis in Eastern India. Sampling was carried out in winter and monsoon seasons between 2013–2015. The objective was to understand whether the isotope composition of the PBM represents source composition. The PBM collected from the waste burning site showed little mass independent fractionation (MIF) ($\Delta^{199}Hg$ = + 0.12 to -0.11‰), similar to the signature in liquid Hg and Hg ores around the world with no seasonal variations. Samples from the industrial site showed mostly negative MDF and MIF ($\delta^{202}Hg$ = -1.34 to -3.48 ‰ and $\Delta^{199}Hg$ = +0.01 to -0.31‰). The MDF is consistent with PBM generated by coal combustion however, the MIF is 0.15‰ more negative compared to the Hg isotope ratios in Indian coals. The traffic junction PBM is probably not produced in situ, but has travelled some distances from nearby industrial sources. The longer residence time of this PBM in the atmosphere has resulted in-aerosol aqueous photoreduction. Thus, the MIF displays a larger range ($\Delta^{199}Hg$ = +0.33 to -0.30‰) compared to the signature from the other sites and with more positive values in the humid monsoon season. Different Hg isotopic signature of PBM in the three different sampling locations within the same city indicates that both source and post emission atmospheric transformations play important roles in determining isotopic signature of PBM.

1. Introduction

Global anthropogenic mercury (Hg) emissions have been exceeding natural emissions since the industrial revolution (Fitzgerald, 1995; Schuster et al., 2002; Fitzgerald et al., 2005). In the past several decades, emerging economies such as China and India have become the major contributors of anthropogenic Hg emissions (UNEP, 2013), as a consequence of increased production of chlorine, metals, waste incineration, coal combustion, cement production and brick manufacturing (Chen et al., 2014). As atmospheric fallouts are

the dominant source of Hg over most of the Earth's surface (Mason et al., 1994; Morel et al., 1998), there is a growing need to quantify atmospheric mercury emission inventories in the Indian subcontinent and China which are home to more than 40% of the global population.

In the atmosphere, Hg exists in two oxidation states, 0 and + 2, and three different operationally defined forms, (G)aseous (E)lemental (M)ercury [GEM; Hg^0], (G)aseous (O)xidized (M)ercury compounds [GOM; Hg^{II}] and (P)articulate/aerosol (B)ound (M)ercury [PBM; $Hg_{(p)}$]. GEM is the dominant form of atmospheric Hg and generally accounts for >95% of total Hg in uncontaminated air (Schroeder and Munthe, 1998; Liu et al., 2010). GEM has a residence time of 0.5–2 years in the atmosphere and is therefore distributed nearly homogenously around the globe. Studies by Weiss-Penzias et al. (2003) indicated that atmospheric emissions of GEM from Asia can be transported across the Pacific within five days. However as GEM has limited solubility in water, it remains largely unavailable to fish and other living organisms. Atmospheric GEM is ultimately oxidized to GOM which is water soluble and contributes towards wet deposition (Lin and Pekhonen, 1999). GEM and GOM can bind to aerosols or particles and the particle bound mercury (PBM) can remain in the atmosphere for several weeks before being deposited locally and regionally. The wet and dry deposition of Hg near a point source is dominated by GOM and PBM, respectively (Lin et al., 2006).

In pristine rural environments, GOM and PBM are typically present in concentrations less than 10 pg/m^3, but in polluted urban-industrial areas and during atmospheric Hg depletion events, their concentration levels can reach in excess of 300 pg/m^3 (Lindberg et al., 2002; Sprovieri et al., 2002; Liu et al., 2010). PBM is largely of anthropogenic origin and can account for up to 40% of total atmospheric Hg in industrialized regions (Xiao et al., 1991). Recent measurements of PBM in several urban/industrial areas have documented that Hg can be associated with large particles (>2.5 μm) and in concentrations similar to those of the vapour phase Hg (ng/m^3) (Hacon et al.,1995; Hladíková et al., 2001; Tsai et al., 2003). GOM and PBM therefore form a significant fraction of the total atmospheric Hg emissions, particularly during coal combustion and municipal waste incineration (Capri, 1996; Pirrone et al., 2001).

A major challenge in source apportionment studies of Hg remains in the fact that it is difficult to identify and quantify different sources once Hg is dispersed and intermixed in the environment (Lindberg et al., 2007). The discovery of mass dependent fractionation (MDF) and mass independent fractionation (MIF) of mercury isotopes (Bergquist and Blum, 2007) have opened up the door to a new method for tracing Hg pollution and investigating Hg behaviour in the environment. Hg has seven stable isotopes (^{196}Hg, ^{198}Hg, ^{199}Hg, ^{200}Hg, ^{201}Hg, ^{202}Hg and ^{204}Hg) out of which the two odd mass isotopes undergo MIF, usually yielding products that are anomalously enriched or depleted in ^{199}Hg and ^{201}Hg (Bergquist and Blum, 2007; Schauble, 2007; Biswas et al., 2008; Ghosh et al., 2008; Carignan et al., 2009; Das et al., 2009, 2013; Laffont et al., 2009; Sherman et al., 2009, 2010, 2012; Sonke, 2011; Chen et al., 2012; Jackson and Muir, 2012, Perrot et al., 2012; Sonke and Blum, 2013). MIF of an isotope of even mass number (^{200}Hg) has also been detected in atmospheric Hg (Gratz et al., 2010; Chen et al., 2012; Sherman et al., 2012, Rolison et al., 2013, Wang et al., 2015) and has been suggested to be caused by photo-induced oxidation of GEM on the surfaces of aerosols and particles in the tropopause (Chen et al., 2012).

To the best of our knowledge, only one study (Rolison et al., 2013) has looked into the Hg isotopic composition of PBM which can form an important component of atmospheric Hg deposition in urban environments. In the present study, Hg isotopic measurements were performed for PM$_{10}$ (particulate matter with size ≤10 micron) samples collected from three locations (a traffic junction, a waste incineration site and an industrial estate) for two seasons, winter and monsoon. The objective of this study was to understand: 1) whether the isotopic composition of the PBM represents the isotopic composition of source, 2) post emission isotopic fractionation during the processes that transport and transform particulate Hg in the atmosphere, and 3) seasonal variation of the isotopic composition of the PBM.

2. Method

2.1 Site description

PBM samples were collected in and around Kolkata (22°32′N, 88°22′E), India in two seasons, winter and monsoon. Kolkata (erstwhile Calcutta) is the capital of West Bengal and is the third most populous city in India according to the 2011 census. The city has a tropical wet and dry climate. The annual mean temperature is 26.8°C with three distinct seasons, summer, monsoon and winter. Winter lasts for about two months between December and January. Temperature starts to rise in the spring months of February to April. The hot and humid summer lasts from May to June with May being the hottest month. Rain lashes the city between June and September brought by the Bay of Bengal branch of the Southwest monsoon. Post monsoon, the temperature cools down during autumn (October–November). Previous studies conducted in different Indian metropolises reported the highest pollutant levels during the cooler months (as the inversion layer remains close to the ground) and the lowest pollutant levels during the monsoon (Chowdhury, 2004; Spiroska et al., 2011; WBPCB, 2012). To capture the seasonal variation of PBM concentrations and isotopic compositions, if any, we specifically collected samples in winter and monsoon seasons between December 2013 and August 2015.

Samples were collected from three locations; a traffic junction, a landfill site and a small industrial town (Figure 1). The traffic junction site is a busy crossing in south Kolkata with no major industries located within a 5 km radius. The landfill site, popularly known as Dhapa dumping ground, is located in the eastern fringe of Kolkata. The disposal site has served the City of Kolkata as an uncontrolled dumping ground since 1981. Little or no soil cover has been applied historically. Although Dhapa does not have any incineration plant, it is a common practice to burn waste in the open air. Waste is also burnt at the Bantala Leather Complex behind Dhapa. These burning practices are in the "unorganised sector". The industrial town, Uttarpara is located in the suburbs of Kolkata, approximately 15 km north of the city on the banks of the River Ganges. There are mainly iron foundries and wagon manufacturing companies in Uttarpara Belt. From the sampling location, several flue gas stacks can be observed. The town is well connected to the city of Kolkata by rail and road. Local trains are the most popular mode of transportation and road traffic in Uttarpara is lesser compared to any traffic junctions in Kolkata.

2.2 Sample collection

A Deployable Particulate Sampler (DPS) pumps (Leland Legacy) with a pumping efficiency of 10 L/min was used to collect the PM_{10}. For each sample the pump ran ~24–50 hours and sampled ~14.4–30 cubic meter air. The PM was collected on 47 mm quartz filters. Prior to the sampling, the quartz filters were dried overnight at 400 °C in an oven, weighed and packed in Millipore petri slides with a cover to prevent any contamination. After sampling, filters were immediately sealed in the petri slides and stored in a refrigerator until analysis.

2.3 Chemical analysis

The filters were weighed before acid digestion to gravimetrically calculate the PM_{10} concentrations. Chemical extraction was carried out within one month of sampling. Depending on PM concentrations, the filters were digested in 8–10 ml, 20% v/v inverse aqua regia (3:1 HNO_3:HCl) in closed Teflon microwave vessels in a Milestone microwave system (ETOS EZ, Italy). The microwave radiation power was 1200 W, the temperature was ramped to 120°C in 15 minutes and then held at 120°C for 30 minutes. The vessels were opened several hours after cooling down to room temperature. The samples were then filtered through 0.22 μm PES membrane filters. Aliquots of the prepared samples were diluted and analysed for Hg and 5 trace metal (Ni, Cu, Zn, As, and Pb) concentrations using an Agilent 7700 series Inductively Coupled Plasma-Mass Spectrometer (ICP-MS Japan) equipped with a 3rd generation He reaction/collision cell (ORS^3) to minimize interferences, particularly formed from the digestion HCl matrix (Das et al., 2015). The operating conditions used for the analysis of samples are shown in Table S1. The ICP-MS operating parameters, such as torch position, sampling depth, extraction and ion focusing lenses voltages, omega lenses voltages, quadrupole settings, and carrier and blend gas flow rates were optimized daily by aspirating a 1.0 μg/L solution of Ce, Co, Li, Mg, Tl and Y in 2 wt % HNO_3. Oxides and doubly charged ion ratios were kept below 2%. The ^{201}Hg isotope was measured, as it is free from polyatomic overlap of WO. Detection Limit (DL) and Background Equivalent

Concentration (BEC) for ^{201}Hg were 7.5 ppt and 42 ppt respectively. HNO_3 and HCl (ultrapure grade) used in the experiment were purchased from J. T. Baker (Canada). Ultra-pure water with 18.2 $MΩ^{-cm}$ resistivity was used (Super-Q; Millipore, USA) for sample and standard preparations.

Hg isotope ratio analyses were performed on a Neptune Plus MC-ICP-MS (Thermo Scientific, Germany) using sample standard (NIST SRM 3133) bracketing technique at the Earth Observatory of Singapore, Nanyang Technological University. The sample solution was reduced to Hg vapour by freshly prepared 3% w/v% $SnCl_2$ in 1 N HCl in a cold vapor hydride generator (CETAC, 200 HGX). Before introduction into the plasma, the Hg vapour was mixed with a dry Tl aerosol (NIST SRM 997, ^{205}Tl/^{203}Tl=2.38714) from a Cetac Aridus II fitted with an ESI nebulizer for instrumental mass bias correction using exponential fractionation law. Typical instrument sensitivity was 200 mV on ^{202}Hg in a 1 ppb NIST SRM 3133 Hg standard with an uptake rate of 350 μl min^{-1} at a 6 rpm pump speed. While measuring the isotope ratios of the samples, total Hg concentrations were also calculated by comparing the signal intensity of ^{202}Hg in 1 ppb bracketing standards with the sample. The total Hg concentrations of the sample extracts were compared to the values obtained by analysing the samples with the Agilent 7700 series ICP-MS. The maximum differences in concentration obtained by these two different methods were ≤12%. The NIST SRM 3133 bracketing standard was prepared in the same matrix (20% v/v, 3:1 HNO_3:HCl) as the samples to avoid any matrix effects.

The isotopes ^{198}Hg, ^{199}Hg, ^{200}Hg, ^{201}Hg, ^{202}Hg, ^{203}Tl, and ^{205}Tl were measured on faraday cups L3, L2, L1, C, H1, H2 and H3, respectively, in static collection mode with a 4 s integration time, and 60 ratios per run. Background corrections were done by beam defocusing. Washout time varied between 5 to 10 minutes until the wash signal stabilized at ≤1% of the preceding measured solution. The MDF of Hg isotopes were expressed as the per mil deviation of the sample relative to the NIST 3133 standard using the delta notation ($δ^xHg$ ‰) and defined by the following equation (Blum and Bergquist, 2007)

$$δ^{xxx}Hg(‰) = ([(^{xxx}Hg/^{198}Hg) \text{ sample} / (^{xxx}Hg/^{198}Hg) \text{ SRM 3133}] - 1) * 1000$$

MIF of Hg isotopes were defined by the deviation from the theoretically predicted MDF and was expressed as (Bergquist and Blum, 2007),

$$Δ^{199}Hg = δ^{199}Hg - 0.252 \text{ x } δ^{202}Hg$$

$$Δ^{200}Hg = δ^{200}Hg - 0.502 \text{ x } δ^{202}Hg$$

$$Δ^{201}Hg = δ^{201}Hg - 0.752 \text{ x } δ^{202}Hg$$

2.4 Blanks, recovery, and uncertainty

A blank filter that was taken to the field was chemically treated in the same way as the samples to determine procedural blank. The total procedural blank, including instrumental background was ≤15 pg and was considered insignificant compared to the amount of Hg extracted from the samples (3.5–10.7 ng). To validate both digestion and ICP-MS methods, blank filters were spiked with Hg standards and treated in the same way as the samples. Recoveries from these spiked filters ranged from 83–96%. The UM-Almaden Hg inter laboratory standard was repeatedly analysed as a secondary standard during the course of analysis. The isotope ratios [$δ^{202}$Hg = –0.55‰ ± 0.14‰, $Δ^{199}$Hg = 0.01‰ ± 0.09‰, and $Δ^{201}$Hg = –0.03‰ ± 0.11‰ (2SD, n = 12)] are identical within errors to the proposed values by Blum and Bergquist (2007) (Table S3). The values of long-term analytical uncertainties of the UM-Almaden were used as uncertainties on sample Hg isotope compositions. However in those samples where triplicate analyses were performed, we reported the uncertainties determined from our own analyses.

3. Results

Table S2 summarizes the trace metal concentrations and Hg isotope compositions of 52 PM_{10} samples, together with background information including sampling period, average temperature, average humidity, PM_{10} concentration, and PBM concentration. Statistical data, e.g. mean, median, 1SD and maximum-minimum values from three locations and in two seasons are reported in Table 1 and Figure 2. For each location and season, $δ^{202}$Hg and $Δ^{199}$Hg are normally distributed (Shapiro-Wilk test). Hence, we use the arithmetic mean and standard deviation to describe the data.

The PBM concentration in the PM_{10} fraction of the air particulates showed a marked decrease in the monsoon season compared to winter. While the average PBM concentrations decreased from 231 ± 51 pg/m^3 (1 SD, n = 4) at the waste incineration site in winter to 158 ± 34 pg/m^3 (1 SD, n = 5) during the monsoon, the values of the traffic junction samples decreased from 408 ± 85 pg/m^3 (1 SD, n = 17) in winter to 369 ± 61 pg/m^3 (1 SD, n = 10) in the monsoon season. The PBM contents in the industrial site samples had a more dramatic decrease from 336 ± 77 pg/m^3 (1 SD, n = 11) in winter to 160 ± 40 pg/m^3 (1 SD, n = 5) during the monsoon. Rainfall can reduce PBM concentrations in two ways. Firstly, precipitation can directly

Table1. Statistical analysis of the PM$_{10}$ concentrations (μg/m^3), PBM concentrations (ng/m^3), δ^{202}Hg, Δ^{199}Hg, Δ^{200}Hg, Δ^{201}Hg (in ‰) measured during the study period

	PBM ng/m^3	PBM ng/m^3	PM$_{10}$ μg/m^3	PM$_{10}$ μg/m^3	δ^{202}Hg‰	δ^{202}Hg‰	Δ^{199}Hg‰	Δ^{199}Hg‰	Δ^{200}Hg‰	Δ^{200}Hg‰	Δ^{201}Hg‰	Δ^{201}Hg‰
Waste	Winter	Monsoon	Winter	Monsoon	Winter	Monsoon	Winter	Monsoon	Winter	Monsoon	Winter	Monsoon
Mean	0.231	0.159	282	210	−0.48	−0.68	0.07	−0.01	0.02	0.03	0.06	0.02
Median	0.231	0.158	289	198	−0.50	−0.72	0.08	−0.02	0.02	0.03	0.04	0.03
SD	0.051	0.034	24	70	0.07	0.10	0.04	0.08	0.00	0.04	0.04	0.07
Skewness	0.01	0.08	−1.3	1.1	0.87	0.97	−0.64	−0.09	−0.66	0.07	1.89	−1.49
Maximum	0.285	0.198	300	321	−0.39	−0.52	0.12	0.09	0.03	0.08	0.11	0.09
Minimum	0.178	0.123	248	132	−0.55	−0.78	0.02	−0.11	0.02	−0.01	0.04	−0.09
N	4	5	4	5	4	5	4	5	4	5	4	5
Industry												
Mean	0.336	0.160	289	190	−2.39	−2.42	−0.18	−0.12	0.04	0.02	−0.16	−0.09
Median	0.331	0.139	318	183	−2.38	−2.48	−0.18	−0.16	0.05	0.04	−0.18	−0.10
SD	0.077	0.040	50	45	0.80	0.57	0.10	0.11	0.04	0.05	0.11	0.11
Skewness	0.88	0.58	−0.33	0.33	−0.11	0.08	0.22	0.37	−0.99	−0.51	0.20	−0.37
Maximum	0.483	0.211	339	250	−1.34	−1.66	−0.02	0.01	0.09	0.07	0.01	0.02
Minimum	0.224	0.122	217	137	−3.48	−3.17	−0.31	−0.24	−0.03	−0.04	−0.32	−0.24
N	11	5	11	5	11	5	11	5	11	5	11	5
Traffic												
Mean	0.408	0.369	352	301	−1.26	−2.03	−0.06	0.10	0.04	0.03	−0.07	0.06
Median	0.419	0.381	361	293	−1.28	−2.25	−0.06	0.06	0.05	0.03	−0.09	0.04
SD	0.085	0.061	61	62	0.84	1.11	0.19	0.16	0.05	0.03	0.19	0.14
Skewness	−0.08	−0.13	−0.02	0.30	−0.42	0.47	0.09	0.03	−0.76	0.08	0.35	0.10
Maximum	0.597	0.468	433	411	−0.12	−0.19	0.20	0.33	0.09	0.09	0.30	0.25
Minimum	0.238	0.276	267	211	−3.06	−3.18	−0.30	−0.16	−0.05	−0.03	−0.29	−0.15
N	17	10	17	10	17	10	17	10	17	10	17	10

doi: 10.12952/journal.elementa.000098.t001

scavenge particulate Hg from the air as evidenced from the large fraction of Hg in rainwater being bound to particles (Munthe, 1993). Secondly, precipitation increases soil humidity, which in turn limits the proportion of wind-blown soil and decreases air particulate concentrations and particulate Hg bound to wind-blown soil material (Fang et. al., 2001). High PM concentrations will likely increase the substrates that Hg can potentially adhere to. Hence, it is not surprising that PM$_{10}$ concentrations correlate with PBM concentrations (R^2= 0.62, Figure S1) as has been observed in other studies (Fang et al., 2001).

PBM is a minor form (~10% of total atmospheric Hg) of anthropogenic Hg, emitted directly to the atmosphere by industrial emissions. It is however often formed by adsorption or partition of gaseous Hg onto a particle surface (Sommar et al., 1997; Brandon et al., 2001). High concentrations of PBM have been reported from many places around the world like Alta Floresta in the Amazon Basin (~100 ng/m^3, Hacon et al.,1995), Beijing (0.360–0.440 ng/m^3, Wang et al., 2002), Taiwan (0.34–5.8 ng/m^3 for PM$_{2.5}$ and 0.05–3.1 ng/m^3 for PM$_{2.5–10}$, Tsai et al., 2003), Detroit (0.12–0.55 ng/m^3, Pirrone et al., 1995), Slovak Republic (0.22–4.47 ng/m^3, Hladíková et al., 2001). PBM concentrations measured in the present study are comparable with those obtained from the Southeast Asian megacities and industrial cities of the West. However, they are far higher than the reported numbers from US, such as Wisconsin (0.0021–0.028 ng/m^3, Lamborg et al., 1995), Florida (0.0049–0.0093 ng/m^3, Guentzel et al., 2001) and are much higher than the background values of 0.001 to 0.086 ng/m^3 (Keeler et al., 1995).

In the present study, 3.36‰ variation in δ^{202}Hg (−3.48 to -0.12‰) and 0.64‰ variation in Δ^{199}Hg (−0.31 to 0.33‰) were observed in the PBM isotope composition (Figure 3). The only other report on PBM isotope compositions is from a coastal environment in Mississippi (Rolison et al., 2013), which showed a much tighter range of δ^{202}Hg (-1.61 to -0.12‰) and a significantly positive Δ^{199}Hg (0.36 to 1.36‰).

On average, δ^{202}Hg was lowest at the industrial site followed by the traffic junction and the waste incineration site in both the seasons. At the industrial site, in winter, average δ^{202}Hg was −2.39 ± 0.80‰, (1SD, n = 11) and during monsoon season, δ^{202}Hg was −2.42 ± 0.57‰ (1SD, n = 5), rendering statistically similar ratios. At the traffic junction, average δ^{202}Hg was −1.26 ± 0.84‰ (1SD, n = 17) and −2.03 ± 1.11‰ (1SD, n = 10)
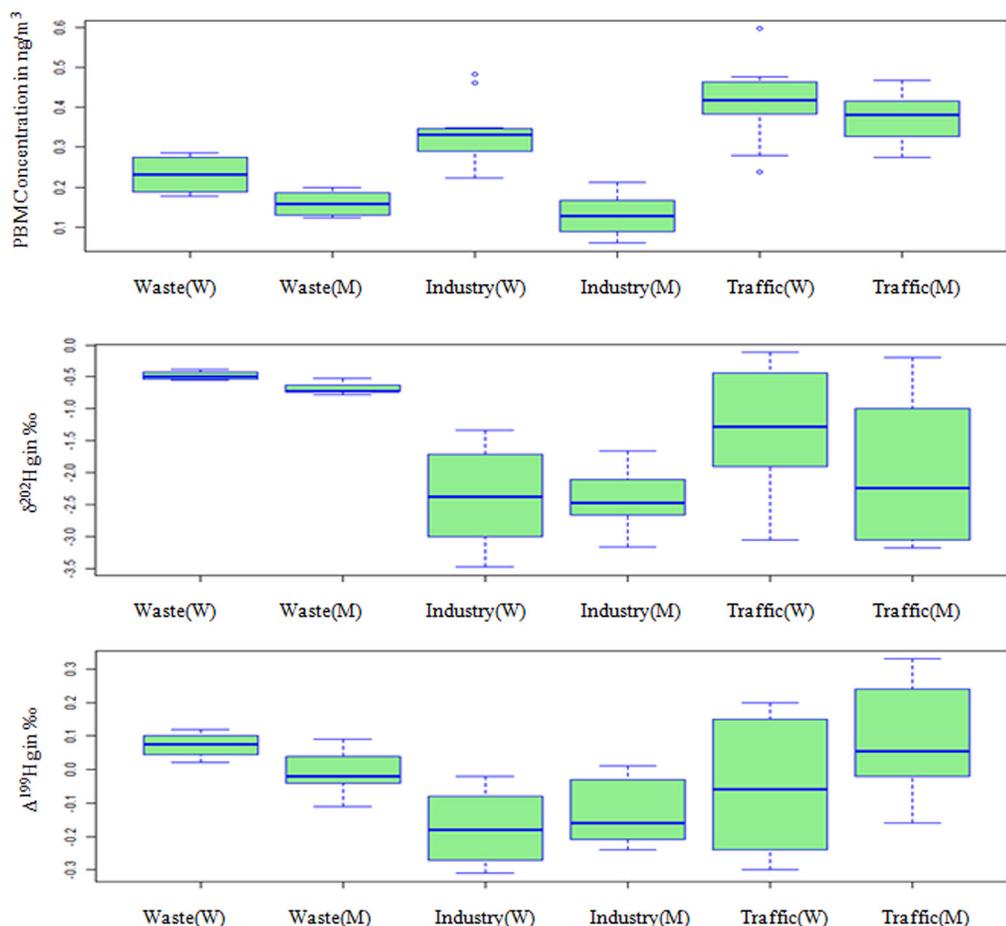
in winter and monsoon, respectively. Compared to the industrial and traffic locations, the waste incineration site showed a much smaller deviation in averaged δ^{202}Hg, –0.48 ± 0.07‰ (1SD, n = 4) in winter and –0.68 ± 0.10‰ (1SD, n = 5) in monsoon. The samples from the waste incineration site showed little to no MIF, with winter average Δ^{199}Hg of 0.07 ± 0.04‰ (1SD, n = 4) and monsoon average Δ^{199}Hg of -0.01 ± 0.08‰ (1SD, n = 5). The industrial site showed slightly negative MIF, with winter average Δ^{199}Hg of -0.18 ± 0.10‰ (1SD, n = 11) and monsoon average Δ^{199}Hg of -0.12 ± 0.11‰ (1SD, n = 5). The traffic junction displayed more variation in MIF with slightly negative MIF in winter (Δ^{199}Hg = -0.06 ± 0.19‰, 1SD, n = 17) and slightly positive MIF in monsoon season (Δ^{199}Hg = 0.10 ± 0.16‰, 1SD, n = 10).

4. Discussion

4.1 Isotopic composition of atmospheric mercury

The Hg isotope signature is a useful tool in understanding sources, tracking specific chemical pathways and monitoring the sinks (Sonke and Blum, 2013). MDF of Hg isotopes can occur in almost all kinetic and equilibrium reactions (Blum et al., 2014). MIF of odd Hg isotopes (Δ^{199}Hg and Δ^{201}Hg) can be triggered by photochemical reduction of Hg(II) and MeHg, aqueous Hg(II)-thiol complexation under equilibrium conditions, evaporation under equilibrium conditions and abiotic dark reduction (Bergquist and Blum, 2007; Zheng et al., 2007; Estrade et al., 2009; Wiederhold et al., 2010; Zheng and Hintelmann, 2010). In combination, MDF and MIF can be a strong tool to track Hg cycle.

Atmospheric Hg composition has been measured in GEM (Demers et al., 2013, Gratz et al., 2010; Rolison et al., 2013, Sherman et al., 2010; Yin et. al., 2013), GOM (Rolison et al., 2013), PBM (Rolison et al., 2013), precipitation (Chen et al., 2012; Demers et. al., 2013; Gratz et al., 2010; Sherman et al., 2012; Wang et al., 2015) and snow (Sherman et al., 2010). Direct measurements of atmospheric GEM showed negative MIF (Δ^{199}Hg from –0.41 to 0.06‰), consistent with the prediction that atmospheric Hg contains complimentary MIF signatures of aquatic reservoirs (Bergquist and Blum, 2007). However GEM samples collected from diverse localities such as Arctic (Sherman et al., 2010), Great Lake Region (Gratz et al., 2010), a semi-rural coastal environment in Mississippi (Rolison et al., 2013), a forest in northeastern Wisconsin, USA (Demers
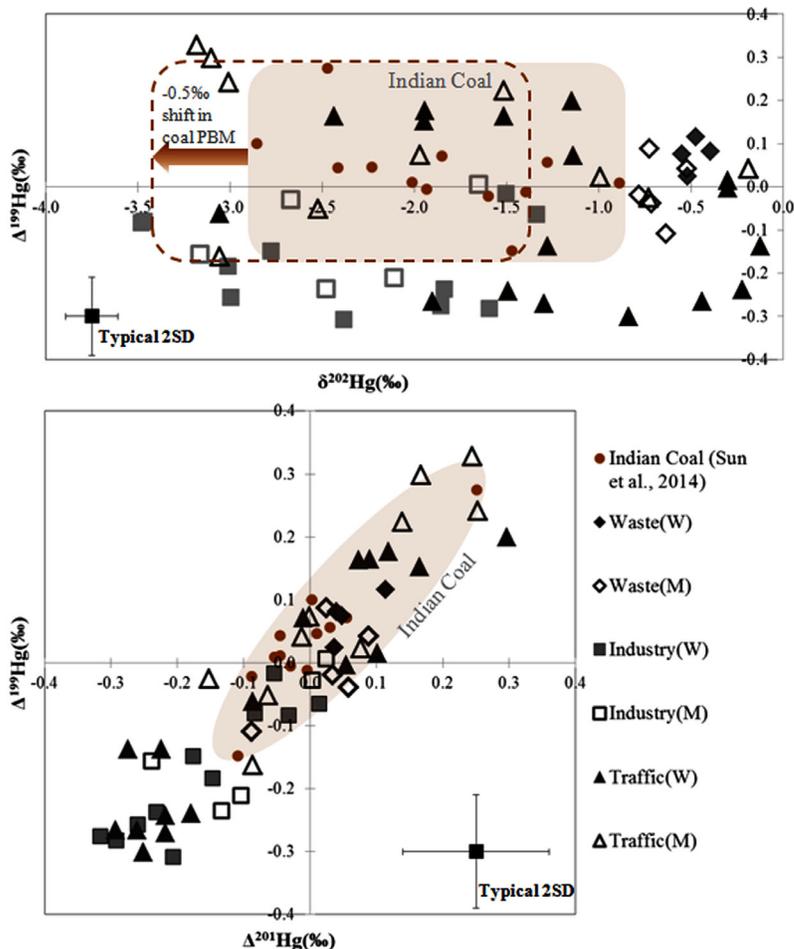
et. al., 2013) and Wanshan mercury mine in Guizhou province, SW China showed a wide range of δ^{202}Hg (−3.88 to +0.93‰). Hg in precipitation has significant positive Δ^{199}Hg ranging from -0.16‰ to +1.16‰ (Demers et. al., 2013; Gratz et al., 2010; Sherman et al., 2010; Chen et al., 2012; Wang et al., 2015) and is thought to be caused by photoreduction in cloud droplets. Recent studies also reported MIF of even Hg isotopes (Δ^{200}Hg) in atmospheric samples, mainly precipitation and snow, that are thought to be triggered by photo-oxidation in the tropopause (Gratz et al., 2010; Chen et al., 2012; Sherman et al., 2012; Wang et al., 2015). However atmospheric Hg isotope composition can be widely variable depending on mixing of different sources and in-source and post-emission fractionation.

The Hg isotope composition of Arctic snow invoked the speculation about the importance of heterogeneous chemistry involving Hg-halogen radical pair intermediates (Sherman et al., 2010). Rain Hg isotope composition stimulated investigations regarding in-cloud photo-reduction and complex reaction mechanisms causing even isotope MIF in upper atmosphere (Chen et al., 2012; Gratz et al., 2010; Sherman et al., 2012; Wang et al., 2015). Measurement of species specific isotope composition of Hg opened up the possibility of measuring Hg isotopes during important atmospheric events like wet and dry deposition (Rolison et al., 2013). As PBM is an important species in urban and polluted environments, isotope fingerprinting of PBM is necessary for an increased understanding of source(s), atmospheric transport and transformation processes.

4.2 Waste incineration

In this study, the sampling location was close to the largest municipal dumping site of the city where open burning of waste is a common practice. During incineration, almost 100% of Hg passes in the flue gas (van Velzen et al., 2002). In waste incineration plants, the flue gas containing particulate matter, heavy metals, sulfur dioxide etc. passes through the flue gas cleaning systems that generally causes isotope fractionation (Sun et al., 2013). However, in the present case, open burning of the wastes results in the emission of atmospheric GEM and particulate Hg with similar isotopic composition as that of the waste, with little to no MIF. The main Hg bearing components in municipal solid wastes are batteries, thermometers and thermostats, pigment and paint residues, fluorescent lamps and dental residues (Kearney & Franklin, 1992). All these components use

Hg extracted from ores. There is evidence for natural fractionation of Hg isotopes in liquid mercury (δ^{202}Hg = -1.06‰ to +0.05‰ and Δ^{199}Hg = -0.05‰ to +0.03‰) (Estrade et al. 2009; Laffont et al., 2011), cinnabar (Hintelmann and Lu, 2003; Stetson et al., 2009) and hydrothermal ores and fluids (Smith et al., 2005, 2008; Sherman et al., 2009). δ^{202}Hg in ore samples can display large variations caused by isotopic fractionation during ore formation (Sherman et al., 2009, Stetson et al., 2009). Statistically significant MIF has not been reported from ore samples. The Hg isotope ratios of PBM measured from the waste incineration site also show small MIF (Δ^{199}Hg = -0.11‰ to +0.12‰). The δ^{202}Hg measured in this study (δ^{202}Hg = -0.78‰ to -0.39‰) is similar to cinnabar ores measured by Stetson et al. (2009) from McDermitt, Nevada (δ^{202}Hg = -0.70‰ to -0.42‰ and Δ^{199}Hg = -0.04‰ to +0.04‰) and liquid Hg isotope composition (Estrade et al., 2009; Laffont et al., 2011). However, more studies are required on Hg isotope compositions of Hg bearing municipal wastes to test this hypothesis.

4.3 Industrial site

The main industries near the sampling location are iron foundries. The foundries mainly cast gray iron. Hence besides coal combustion, the high temperature metal smelting process can be a potential source of Hg. Basic raw materials used by the foundry units are pig iron and different types of scrap excluding automobile parts. Sometimes alloying elements such as nickel, chromium, copper, vanadium, and titanium are added. To test the main source(s) of Hg in the air particulates, we measured several trace metal concentrations as anthropogenic end members have distinct trace metal signatures (Table S2). For example, coal combustion primarily releases arsenic and lead while metal smelting releases copper, zinc, chromium and nickel, among others (Pacyna, 1987). In our study, Hg shows strong correlation with As (0.74) and Pb (0.71) (Table S4), which indicates the major source to be coal combustion (Pacyna et al., 2010).

To mitigate the effect of long-range transport of PBM from the roads in the urban area to the suburban industrial areas, the sampling pump in the industrial site was placed within close proximity (several hundred meters) of the flue gas stacks. The industry management informed that 70% of the feed coal comes from the local coal fields whereas the rest 30% is Australian coal. Mercury isotopes can be a reliable tool to trace the Hg emissions from coal combustion, because coal from different geographical regions typically has distinctive Hg isotopic signatures (Sun et al., 2014), and there is a small and predictable isotopic fractionation between feed coal and bulk flue gas emissions (Sun et al., 2013). Sun et al. (2014) proposed a double Rayleigh isotope fractionation model to predict speciated coal Hg isotope emissions. Based on their model, δ^{202}Hg can shift by -0.5‰ for emitted PBM relative to the feed coal. The most fractionated δ^{202}Hg of Indian coal reported so far is -2.86‰ (Sun et al., 2014). This will generate PBM with δ^{202}Hg of -3.36‰ which within analytical uncertainty, is consistent with the measured number of the most fractionated PBM sample from the industrial site (Figure 3). Δ^{199}Hg of Indian coal shows a large range from +0.28‰ to -0.15‰ (Sun et al., 2014) with most of the samples concentrating around 0. However, none of the Hg species in the stack emission produce MIF. Hence, GEM, GOM and PBM from coal combustion can retain a similar MIF signature as that of feed coal. Δ^{199}Hg of PBM collected from the industrial sites in this study overlapped the range expected for Indian coal with several samples showing up to -0.31‰ MIF. Post emission in cloud photoreduction would cause a positive shift in the observed Δ^{199}Hg. Therefore, the -0.15‰ shift of the few PBM samples from the feed coal isotope values cannot be explained by post emission reactions in the atmosphere. We speculate that the sampled PBM have two sources, Indian coal and a second source which has more negative Δ^{199}Hg. The second source could be either Australian Coal or background GEM adhering to PM_{10}, or combination of both. As we do not have any information on the Hg isotope ratios of Australian coal, we cannot predict a mixing model for PBM isotopes from the two different feed coals. However previous studies have reported negative Δ^{199}Hg in GEM, up to -0.4‰ (Rolison et al., 2013). Assuming a simple binary mixing model, 60% of the most fractionated GEM (Δ^{199}Hg = -0.4‰) adhering to PM_{10} mixed with 40% of PBM emitted by the most fractionated Indian coal (Δ^{199}Hg = -0.15‰) can produce PBM Δ^{199}Hg of -0.3‰. In absence of exact feed coal data and isotopic composition of background GEM, we interpret that the overall observed PBM isotopic composition in the industrial site samples is broadly consistent with coal combustion emission models proposed by Sun et al. (2014).

4.4 Traffic junction

The Hg content in gasoline is much lower (Conaway et al., 2005; Won et al., 2007) compared to coal (Yudovich and Ketris, 2005). Studies show that both in idling and driving modes, the automobile exhaust gas mainly contains GEM with no detectable levels of PBM or GOM (Won et al., 2007). As road transport is considered the dominant source of PM_{10} (Senaratne et al., 2005), we envisage the high concentrations of PBM in the traffic junction samples are due to availability of PM that forms the substrate for GEM + GOM to adhere. The waste incineration site is within 5 km radius of the traffic junction and there are numerous small and medium scale industries within 10 km radius. Hence the traffic junction PBM source is likely mixed between traffic emission, coal combustion, waste incineration and re-emission of previously deposited road dust.

The PBM isotope composition of traffic junction samples shows a wide range and cannot be attributed to one source. Hg only moderately correlates with As (0.55) (Table S4), indicating coal combustion to be at least one of the sources. However, as Hg does not correlate with any of the other trace metals measured in this study, the sources remain inconclusive. δ^{202}Hg has a ~3‰ range and Δ^{199}Hg varies from +0.33 to -0.30‰. The only published isotope study on PBM reported similar δ^{202}Hg ratios from -1.61‰ to -0.12‰, however, the MIF was strongly positive with Δ^{199}Hg ranging from +0.36‰ to +1.27‰ (Rolison et al., 2013). Rolison et al. explained the observed MDF by coal combustion supported by air mass back trajectory analysis and the positive MIF by in-aerosol photoreduction. PM_{10} can be composed of non-hygroscopic material like dust, fly ash, carbon and hygroscopic sulphate, nitrate and sea salt (ten Brink et al., 1997). In the monsoon season, the Southwest Monsoon winds originating in the Bay of Bengal blow over the city. Hence, the presence of hygroscopic components in the PM_{10} combined with a high relative humidity can trigger aqueous photo reduction reactions (Bergquist and Blum, 2007) in minute scale within the aerosol leaving the aerosols enriched in odd MIF. In addition, the PBM in the traffic junction is envisaged to have travelled a longer distance with a longer atmospheric residence time as compared to the PBM collected in the industrial and waste burning sites. Therefore, in situ atmospheric redox reactions are more likey to occur in PBM samples from the traffic junction site. We therefore consider the large spread in MIF in our data caused by a combination of retention of original source signature and in aerosol photo reduction.

4.5 Seasonal variation

Statistical tests were performed in order to understand whether the winter and monsoon isotope ratios (δ^{202}Hg and Δ^{199}Hg) differ significantly at the industrial site and traffic junction. As there are too few data points for the waste incineration site for both seasons, the tests could not be performed for those samples. The nonparametric Mann-Whitney-Wilcoxon test was first performed to check whether there is any seasonal variation of δ^{202}Hg and Δ^{199}Hg in the industrial site and traffic junction. This test gave statistically significant evidence (p-value = 0.04, at 0.05 significant level) only for the Δ^{199}Hg in the traffic junction. To further investigate whether the difference in the winter and monsoon Δ^{199}Hg in the traffic junction is real, their descriptive statistics were analysed (Table 1). We note that the mean values are -0.06‰ in winter versus 0.1‰ in monsoon. Since the skewness of Δ^{199}Hg of the traffic junction for both the seasons was low (winter data = 0.09 and monsoon data =0.03), it is assumed that the distributions are reasonably close to normal, thus allowing the two sample t-Test to be conducted. The results of the t-Test (t = -2.28, df = 21.1, p-value = 0.03) lead to a conclusion that mean values of the winter and monsoon data are significantly different at the 0.05 significance level. The boxplots of the winter and monsoon data (Figure 2) also illustrate the median Δ^{199}Hg of the monsoon season to be higher than the winter. On the basis of the above discussion, it is concluded that the mean as well as the median of Δ^{199}Hg is higher in monsoon vis-à-vis winter in the traffic junction.

The average humidity during the monsoon season is high, increasing the scope of in aerosol photoreduction in the hydroscopic PM_{10} particles. This can leave the PBM enriched in the odd isotopes (Gratz et al., 2010). We also see a moderate correlation between humidity and Δ^{199}Hg (R^2 = 0.55) in the traffic junction site for monsoon season strengthening our hypothesis. Residence time of PBM in the atmosphere also possibly plays a significant role in post emission atmospheric transformations. Higher values of Δ^{199}Hg were not seen in the industrial and waste burning site during the monsoon season as they were collected near the point source. Hence, the residence time of PBM in the atmosphere was significantly shorter than that in the traffic junction.

5. Conclusion

We have reported for the first time the Hg isotopic composition of PBM in PM_{10} from near point sources of emission; a traffic junction, a waste burning site and an industrial site in and around heavily polluted Kolkata. All samples displayed negative MDF, while the MIF varied between -0.31‰ to +0.33‰. Within the same city, the industrial, waste incineration and urban traffic site revealed different PM_{10} Hg isotope signatures. The results demonstrated that the PBM isotopic composition in the industrial site overall fits the model predicting coal combustion emission (Sun et al., 2014). Though we do not know the Hg isotopic composition of bulk municipal waste, we assume it is similar to that of Hg ore and liquid Hg with practically zero MIF. The PBM emitted by open burning also showed very little MIF. The traffic junction PBM showed a larger variation within one season and also across seasons. Though vehicular emission is the single largest source of PM in urban air, it is not a major source of PBM. Hence the high PBM measured in the traffic junction is possibly due to scavenging of background GOM and GEM by the plentiful air particulates. The back ground GOM and GEM in the city air come from numerous industries around the city and waste burning. The residence time and distance travelled is higher than the PBM at the other two sampled sites. Hence the original isotopic signature of the source can be modified by atmospheric processes which are the likely cause for the larger spread in isotope ratios. Moreover, PM_{10} composition is different in two seasons. While the winter PM_{10} composition is dominated by dust blowing from the north, the monsoon PM_{10} can be dominated by hydroscopic particles such as sea salt when the air mass blows from over the Bay of Bengal.

Hence in aerosol, aqueous photoreduction might be more dominant during the monsoon season resulting in statistically slightly higher mean positive MIF as compared to winter data. In summary, this study shows that isotopic composition of PBM can be a powerful tool to determine point sources. However, atmospheric reactions can modify the source signature if the PBM has a considerable long residence time in the atmosphere and/or it has travelled long distances prior to deposition.

References

Bergquist BA, Blum JD. 2007. Mass-dependent and -independent fractionation of Hg isotopes by photoreduction in aquatic systems. *Science* **318**: 417–420.

Biswas A, Blum JD, Bergquist BA, Keeler GJ, Xie Z. 2008. Natural mercury isotopes variation in coal deposits and organic soils. *Environ Sci Technol* **42**: 8303–8309.

Blum JD, Bergquist BA. 2007. Reporting of variations in the natural isotopic composition of mercury. *Anal Bioanal Chem* **388**: 353–359.

Blum JD, Sherman LS, Johnson MW. 2014. Mercury isotopes in earth and environmental sciences. *Annu Rev Earth Planet Sci* **42**: 249–269.

Brandon NP, Francis PA, Jeffrey J, Kelsall GH, Yin Q. 2001. Thermodynamics and electrochemical behaviour of Hg–S–Cl–H2O systems. *J Electroanal Chem* **497**: 18–32.

Capri A. 1996. Mercury from combustion sources: A review of the chemical species emitted and their transport in the atmosphere. *Water Air Soil Pollut* **98**: 241–254.

Carignan J, Estrade N, Sonke JE, Donard OFX. 2009. Odd isotope deficits in atmospheric Hg measured in lichens. *Environ Sci Technol* **43**: 5660–5664.

Chen J, Hintelmann H, Feng X, Dimock B. 2012. Unusual fractionation of both odd and even mercury isotopes in precipitation from Peterborough, ON, Canada. *Geochim Cosmochim Acta* **90**: 33–46.

Chen L, Wang HH, Liu JF, Tong YD, Ou LB, et al. 2014. Intercontinental transport and deposition patterns of atmospheric mercury from anthropogenic emissions. *Atmos Chem Phys* **14**: 10163–10176.

Chowdhury MZ. 2004. Characterization of Fine Particle Air Pollution in the Indian Subcontinent. *PhD Thesis*. Georgia, United States: Georgia Institute of Technology. 201 pages.

Conaway CH, Mason RP, Steding DJ, Flegal AR. 2005. Estimate of mercury emission from gasoline and diesel fuel consumption, San Francisco Bay Area, California. *Atmos Environ* **39**: 101–105.

Das R, Bizimis M, Wilson AM. 2013. Tracing mercury seawater vs atmospheric inputs in a pristine SE USA salt marsh system: Mercury isotope evidence. *Chem Geol* **336**: 50–61.

Das R, Khezri B, Srivastava B, Datta S, Sikdar PK, et al. 2015. Trace Element Composition of $PM_{2.5}$ and PM_{10} from Kolkata - A Heavily Polluted Indian Metropolis. *Atmos Pollut Res* **6**: 742–750.

Das R, Salters VJM, Odom AL. 2009. A case for in vivo mass-independent fractionation of mercury isotopes in fish. *Geochem Geophys Geosyst* **10**. doi: 10.1029/2009GC002617.

Demers JD, Blum JD, Zak DR. 2013. Mercury isotopes in a forested ecosystem: Implications for air-surface exchange dynamics and the global mercury cycle. *Global Biogeochem Cy* **27**: 222–238. doi: 10.1002/gbc.20021.

Estrade N, Carignan J, Sonke JE, Donard OFX. 2009. Mercury isotope fractionation during liquid-vapor evaporation experiments. *Geochim Cosmochim Acta* **73**: 2693–2711.

Fang F, Wang Q, Liu R, Ma Z, Hao Q. 2001. Atmospheric particulate mercury in Changchun City, China. *Atmos Environ* **35**: 4265–4272.

Fitzgerald WF. 1995. Is mercury increasing in the atmosphere? The need for an atmospheric mercury network (AMNET). *Water Air Soil Pollut* **80**: 245–254.

Fitzgerald WF, Engstrom DR, Lamborg CH, Tseng CM, Balcom PH, et al. 2005. Modern and historic atmospheric mercury fluxes in northern Alaska: Global sources and Arctic depletion. *Environ Sci Technol* **39**: 557–568.

Ghosh S, Xu Y, Humayun M, Odom AL. 2008. Mass-independent fractionation of mercury isotopes in the environment. *Geochem Geophys Geosyst* **9**. doi: 10.1029/2007GC001827.

Gratz LE, Keeler GJ, Blum JD, Sherman LS. 2010. Isotopic composition and fractionation of mercury in Great Lakes precipitation and ambient air. *Environ Sci Technol* **44**: 7764–7770.

Guentzel JL, Landing WM, Gill GA, Pollman CD. 2001. Processes influencing rainfall deposition of mercury in Florida. *Environ Sci Technol* **35**: 863–873.

Hacon S, Artaxo P, Gerab F, Yamasoe MA, Campos RC, et al. 1995. Atmospheric mercury and trace elements in the region of Alta Floresta in the Amazon Basin. *Water Air Soil Pollut* **80**: 273–283.

Hintelmann H, Lu SY. 2003. High precision isotope ratio measurements of mercury isotopes in cinnabar ores using multi-collector inductively coupled plasma mass spectrometry. *Analyst* **128**: 635–639.

Hladíková V, Petrík J, Jursa S, Ursínyová M, Kočan A. 2001. Atmospheric mercury levels in the Slovak Republic. *Chemosphere* **45**: 801–806.

Jackson TA, Muir DCG. 2012. Mass-dependent and mass-independent variations in the isotope composition of mercury in a sediment core from a lake polluted by emissions from the combustion of coal. *Sci Total Environ* **417–418**: 189–203.

Kearney AT & Franklin Associates, Inc. (contractors). 1992. Characterisation of products containing mercury in muncipal solid waste in the United States, 1970-2000, EPA contract No 68-W9-0040. *Final report issued as US EPA Report 530-R-92-013*. Washington DC.

Keeler GJ, Glinsorn G, Pirron N. 1995. Particulate mercury in the atmosphere: Its significance, transformation and sources. *Water Air Soil Pollut* **80**: 159–168.

Laffont L, Sonke JE, Maurice L, Hintelmann H, Pouilly M, et al. 2009. Anomalous mercury isotopic compositions of fish and human hair in the Bolivian Amazon. *Environ Sci Technol* **43**: 8985–8990.

Laffont L, Sonke JE, Maurice L, Monrroy SL, Chincheros J, et al. 2011. Hg speciation and stable isotope signatures in human hair as a tracer for dietary and occupational exposure to mercury. *Environ Sci Technol* **45**: 9910–9916.

Lamborg CH, Fitzgerald WF, Vandal GM, Rolfus KR. 1995. Atmospheric mercury in northern Wisconsin: Sources and species. *Water Air Soil Pollut* **80**: 189–198.

Lin C-J, Pehkonen SO. 1999. The chemistry of atmospheric mercury: A review. *Atmos. Environ.* **33**: 2067–2079.

Lin C-J, Pongprueksa P, Lindberg SE, Pehkonen SO, Byun D, et al. 2006. Scientific uncertainties in atmospheric mercury models i: Model science evaluation. *Atmos Environ* **40**: 2911–2928.

Lindberg S, Bullock R, Ebinghaus R, Engstrom D, Feng X, et al. 2007. A synthesis of progress and uncertainties in attributing the sources of mercury in deposition. *Ambio* **36**: 19–32.

Lindberg SE, Brooks S, Lin CJ, Scott KJ, Landis MS, et al. 2002. Dynamic oxidation of gaseous mercury in the Arctic troposphere at polar sunrise. *Environ Sci Technol* **36**: 1245–1256.

Liu B, Keeler GJ, Dvonch T, Barres JA, Lynam MM, et al. 2010. Urban–rural differences in atmospheric mercury speciation. *Atmos Environ* **44**: 2013–2023.

Mason RP, Fitzgerald WF, Morel FMM. 1994. The biogeochemical cycling of elemental mercury: Anthropogenic influences. *Geochim Cosmochim Acta* **58**: 3191–3198.

Morel FMM, Kraepiel AML, Amyot M. 1998. The chemical cycle and bioaccumulation of mercury, *Annu Rev Ecol Syst* **29**: 543–566.

Munthe J. 1993. Report prepared for the Workshop on Emission and Modeling of Persistent Organic Pollutants and Heavy Metals. Durham, Carolina.

Pacyna JM. 1987. Atmospheric emissions of arsenic, cadmium, lead and mercury from high temperature processes in power generation and industry, in Hutchinson TC, Meema KM, eds.,   *Lead, Mercury, Cadmium and Arsenic in the Environment*. Chichester, Wiley: pp. 69–87.

Pacyna JM, Pacyna EG, Aas W. 2010. Changes of emissions and atmospheric deposition of mercury, lead, and cadmium, Fifty Years of Endeavour. *Atmos Environ* **43**: 117–127.

Perrot V, Pastukhov MV, Epov VN, Husted S, Donard OFX, et al. 2012. Higher mass-independent isotope fractionation of methylmercury in the pelagic food web of Lake Baikal (Russia). *Environ Sci Technol* **46**: 5902–5911.

Pirrone N, Costa P, Pacyna JM, Ferrara R. 2001. Mercury emissions to the atmosphere from natural and anthropogenic sources in the Mediterranean region. *Atmos Environ* **35**: 2997–3006.

Pirrone N, Glinsorn G, Keeler GJ. 1995. Ambient levels and dry deposition fluxes of mercury to Lakes Huron, Erie and St Clair. *Water Air Soil Pollut* **80**: 179–188.

Rolison JM, Landing WM, Luke W, Cohen M, Salters VJM. 2013. Isotopic composition of species-specific atmospheric Hg in a coastal environment. *Chem Geol* **336**: 37–49.

Schauble EA. 2007. Role of nuclear volume in driving equilibrium stable isotope fractionation of mercury, thallium, and other very heavy elements. *Geochim Cosmochim Acta* **71**: 2170–2189.

Schroeder WH, Munthe J. 1998. Atmospheric mercury—an overview. *Atmos Environ* **32**: 809–822.

Schuster PF, Krabbenhoft DP, Naftz DL, Cecil LD, Olson ML, et al. 2002. Atmospheric mercury deposition during the last 270 years: A glacial ice core record of natural and anthropogenic sources. *Environ Sci Technol* **36**: 2303–2310.

Senaratne I, Kelliher FM, Triggs C. 2005. Source Apportionment of Airborne Particles during Winter in Contrasting, Coastal Cities. *Aerosol Air Qual Res* **5**: 48–64.

Sherman LS, Blum JD, Johnson KP, Keeler GJ, Barres JA, et al. 2010. Mass-independent fractionation of mercury isotopes in Arctic snow driven by sunlight. *Nat Geosci* **3**: 173–177.

Sherman LS, Blum JD, Keeler GJ, Demers JD, Dvonch JT. 2012. Investigation of local mercury deposition from a coal-fired power plant using mercury isotopes. *Environ Sci Technol* **46**: 382–390.

Sherman LS, Blum JD, Nordstrom DK, McCleskey RB, Barkay T, et al. 2009. Mercury isotopic composition of hydrothermal systems in the Yellowstone Plateau volcanic field and Guaymas Basin sea-floor rift. *Earth Planet Sci Lett* **279**: 86–96.

Smith CN, Kesler SE, Blum JD, Rytuba JJ. 2008. Isotope geochemistry of mercury in source rocks, mineral deposits and spring deposits of the California Coast Ranges, USA. *Earth Planet Sci Lett* **269**: 399–407.

Smith CN, Kesler SE, Klaue B, Blum JD. 2005. Mercury isotope fractionation in fossil hydrothermal systems. *Geology* **33**: 825–828.

Sommar J, Hallquist M, Ljungstrom E, Lindqvist O. 1997. On the gas phase reactions between volatile biogenic mercury species and the nitrate radical. *J Atmos Chem* **27**: 233–247.

Sonke JE. 2011. A global model of mass independent mercury stable isotope fractionation. *Geochim Cosmochim Acta* **75**: 4577–4590.

Sonke JE, Blum JD. 2013. Advances in mercury stable isotope biogeochemistry. *Chem Geol* **336**: 1–4.

Spiroska J, Rahman MA, Pal S. 2011. Air pollution in Kolkata: An analysis of current status and interrelation between different factors. *SEEU Review* **8**: 182–214.

Sprovieri F, Pirrone N, Hedgecock IM, Landis MS, Stevens RK. 2002. Intensive atmospheric mercury measurements at Terra Nova Bay in Antarctica during November and December 2000. *J Geophys Res* **107**: doi: 10.1029/2002JD002057.

Stetson SJ, Gray JE, Wanty RB, Macalady DL. 2009. Isotopic variability of mercury in ore, mine-waste calcine, and leachates of mine-waste calcine from areas mined for mercury. *Environ Sci Technol* **43**:7331–7336.

Sun R, Heimbürger L-E, Sonke JE, Liu G, Amouroux D, et al. 2013. Mercury stable isotope fractionation in six utility boilers of two large coal-fired power plants. *Chem Geol* **336**: 103–111.

Sun R, Sonke J, Heimbürger L-E, Belkin H, Liu G, et al. 2014. Mercury stable isotope signatures of world coal deposits and historical coal combustion emissions. *Environ Sci Technol* **48**: 7660–7668.

ten Brink HM, Kruisz C, Kos GPA, Berner A. 1997. Composition/size of the light-scattering aerosol in the Netherlands. *Atmos Environ* **31**: 3955–3962.

Tsai Y, Kuo S, Lin Y. 2003. Temporal characteristics of inhalable mercury and arsenic aerosols in the urban atmosphere in southern Taiwan. *Atmos Environ* **37**: 3401–3411.

UNEP (United Nations Environment Programme). 2013. Global Mercury Assessment 2013: Sources, Emissions, Releases and Environmental Transport. Geneva, Switzerland: UNEP Chemicals Branch.

van Velzen D, Langenkamp H, Herb G. 2002. Review: Mercury in waste incineration. *Waste Manage Res* **20**: 556–568.

Wang W, Liu J, Yang S, Peng A. 2002. Distribution of mercury on the aerosol in the atmosphere of Beijing. *J Shanghai Jiaotong Univ (China)* **36**: 134–137.

Wang Z, Chen J, Feng X, Hintelmann H, Yuan S, et al. 2015. Mass-dependent and mass-independent fractionation of mercury isotopes in precipitation from Guiyang, SW China. *C R Geosci*. doi: 10.1016/j.crte.2015.02.006.

WBPCB (West Bengal Pollution Control Board). 2012. A Report on Trend of Important Air Quality Parameters in Kolkata during Night Time as Compared to Daytime Situation during Year 2011 and 2012. 61 pages.

Weiss-Penzias P, Jaffe DA, McClintick A, Prestbo EM, Landis MS. 2003. Gaseous elemental mercury in the marine boundary layer: Evidence for rapid removal in anthropogenic pollution. *Environ Sci Technol* **37**: 3755–3763.

Wiederhold JG, Cramer CJ, Daniel K, Infante I, Bourdon B, et al. 2010. Equilibrium mercury isotope fractionation between dissolved Hg(II) species and thiol-bound Hg. *Environ Sci Technol* **44**: 4191–4197.

Won JH, Park JY, Lee TG. 2007. Mercury emissions from automobiles using gasoline, diesel, and LPG. *Atmos Environ* **41**: 7547–7552.

Xiao ZF, Munthe J, Schroeder WH, Lindqvist O. 1991. Sampling and determination of gaseous and particulate mercury in the atmosphere using gold-coated denuders. *Water Air Soil Pollut* **55**: 141–151.

Yin R, Feng X, Meng B. 2013. Stable mercury isotope variation in rice plants (*Oryza sativa* L.) from the Wanshan mercury mining district, SW China. *Environ Sci Technol* **47**: 2238–2245.

Yudovich YE, Ketris MP. 2005. Mercury in coal: A review: Part 1. Geochemistry. *Int J Coal Geol* **62**: 107–134.

Zheng W, Foucher D, Hintelmann H. 2007. Mercury isotope fractionation during volatilization of Hg (0) from solution into the gas phase. *J Anal Atom Spectrom* **22**: 1097–1104.

Zheng W, Hintelmann H. 2010. Nuclear field shift effect in isotope fractionation of mercury during abiotic reduction in the absence of light. *J Phys Chem A* **114**: 4238–4245.

Contributions

- Contributed to conception and design: RD, XW, RDW, PKS
- Contributed to acquisition of data: RD, XW, BK, PKS
- Contributed to analysis and interpretation of data: All authors
- Drafted and/or revised the article: RD, XW, RDW, SD
- Approved the submitted version for publication: All authors

Acknowledgments

Funding information

Competing interests

We declare that we have no competing interests.

Supplemental material

- **Table S1. Agilent 7700 ICP-MS operating conditions for the analysis of PBM samples. (DOC)**
  doi: 10.12952/journal.elementa.000098.s001
- **Table S2. PBM sampling details along with the isotope ratios and trace metal concentrations. (XLX)**
  doi: 10.12952/journal.elementa.000098.s002
- **Table S3. Isotope ratios of 1.2 ppb UM-Almaden standard measured during the course of analyses. (DOC)**
  doi: 10.12952/journal.elementa.000098.s003
- **Table S4. Correlation coefficients (r) among trace metals and PBM in PM_{10} from industrial site and traffic junction. (DOC)**
  doi: 10.12952/journal.elementa.000098.s004
- **Figure S1. Plot showing PBM concentration (ng/m^3) vs. PM_{10} concentrations ($\mu g/m^3$).**

  The PBM was collected in two seasons, winter and monsoon from three locations, waste incineration site, industrial site and traffic junction (n = 52). (DOC) doi: 10.12952/journal.elementa.000098.s005

Data accessibility statement

All data are included within this manuscript.

Copyright